Mechanism and Machine Theory 120 (2018) 73–88

Contents lists available at ScienceDirect

Mechanism and Machine Theory

journal homepage: www.elsevier.com/locate/mechmachtheory

Research paper

Stiffness and mass optimization of parallel kinematic machine

Tao Sun[a], Binbin Lian[a,b,*]

[a] Key Laboratory of Mechanism Theory and Equipment Design of Ministry of Education, Tianjin University, Tianjin 300350, China
[b] Department of Machine Design, School of Industrial Engineering and Management, KTH Royal Institute of Technology, Stockholm 10044, Sweden

ARTICLE INFO

Article history:
Received 18 July 2017
Revised 6 September 2017
Accepted 17 September 2017
Available online 28 September 2017

Keywords:
Parallel kinematic machine (PKM)
Multi-objective optimization
Analytical mapping model
Probabilistic constraints
Pareto frontier
Cooperative equilibrium point

ABSTRACT

It has long been a challenge to carry out the optimal design of parallel kinematic machine (PKM) simultaneously considering stiffness and mass performances. This paper proposes the stiffness and mass optimization of PKM by settling performance indices, constraint conditions based on parameter uncertainty and cooperative equilibrium among performances. Firstly, instantaneous energy-based stiffness indices and mass in motion are defined as objectives. Instead of computationally expensive numerical analysis, analytical mapping models between objectives and parameters are investigated to improve optimization efficiency. Then, considering the effects of parameter uncertainty resulted from manufacturing errors during construction, constraint conditions are formulated by probabilistic method. Based on particle swarm optimization (PSO), a multi-objective optimization is implemented. A group of solutions are obtained to flag as Pareto frontier that reflects the competitive features between stiffness and mass performances. A cooperative equilibrium searching method is proposed to find out the final solution. Finally, this optimization approach is exemplified and validated by a five degree-of-freedom (DoF) PKM. Although its mass increases 17.17%, the stiffness is nearly 3 times better than before optimization.

1. Introduction

Parallel kinematic machine (PKM) consists of moving platform, fixed base and at least two kinematic chains [1–4]. It can be designed as compact module and applied to form parallel or hybrid machine tool by integrating with articulated heads or long guideways. PKM has desirable performances in accuracy and rigidity as traditional machines, and in workspace/footprint ratio, dynamic response and flexibility as articulated serial robots [5,6]. It has been recognized as promising solution for machine tools [7,8], telescope positioning [9] and food packaging [10] etc. Although PKMs have found the market in many applications, they are not as successful as expected. Most existing PKMs are expensive devices that provide worse performances than conventional machines. Further investigation is necessary for making PKM more attractive to industries. Among the main issues to be addressed, the optimal design problem is crucial [11].

The purpose of optimal design aims at enhancing performance indices by adjusting dimensional or sectional parameters of PKMs. These parameters should satisfy certain constraints, such as limitation of workspace or maximum errors. Then the parameter adjustment is implemented by optimization algorithm [12]. This approach is called performance optimization of PKMs. In the optimization process, two basic and important performances are usually involved, i.e. stiffness and mass. The former is directly related to machining deformation and accuracy, while the latter affects dynamic performance.

* Corresponding author.
E-mail address: lianbinbin@tju.edu.cn (B. Lian).

https://doi.org/10.1016/j.mechmachtheory.2017.09.014
0094-114X/

In the past few decades, optimization of PKMs towards high stiffness has been intensively reported. For instance, Kang [13] defined stiffness metric by using weighted sum of stiffness along different directions, and carried out manipulability and stiffness optimal design of a two degree-of-freedom (DoF) PKM. Bi [14] formulated stiffness matrix of Tripod PKM by Jacobian matrix and then performed its optimization taking weighted objective among stiffness, workspace, dexterity and purity as the optimal function. Shin defined a weighted factor by multiplying the determinant and isotropy of stiffness matrix. He then regarded the weighted sum as single objective function to optimize a redundant PKM [15]. The diagonal elements of stiffness matrix are applied as the objective function to implement stiffness optimal design of 3-DoF and 6-DoF PKMs [12,16].

It is noted from above literature that increasing parameter values benefits the stiffness enhancement. But it will have a negative influence on the dynamic performance of PKMs by enlarging the scale and increasing the weight. Therefore, stiffness and mass performances are competitive and restrain each other. By regarding any of them as the single objective in the optimal design process, the performance optimization becomes a game that two players (stiffness and mass) act according to their own strategies to maximize their individual gains [17]. The resulting solution cannot reach the best interest for both since the players act independently without cooperating with each other [18]. A cooperative play is necessary to deal with optimization of stiffness and mass performances.

There have been two ways to incorporate both stiffness and mass performances into the optimization of PKMs. The first way is regarding natural frequency as objective function. Being formulated by the ratio of stiffness and mass, natural frequency has the merits of unit invariance and clear physical meaning [19,20]. Menon obtained optimal geometric parameters of PKMs with US and UPS kinematic chains through maximizing the first natural frequency in prescribed workspace [21]. Herein, P, U and S denote prismatic, universal and spherical joints. Similarly, Alessandro determined optimal geometric parameters of a 4-DoF PKM by maximizing natural frequency when moving platform is at a fixed pose and within a cube workspace [22]. Although natural frequency is helpful in obtaining a stiffer PKM with lightweight structure, the cooperative game between stiffness and mass performances become a single objective optimization. Ratio of stiffness and mass is to be maximized instead of searching for their best compromise. It might lead to that solutions hidden in concavities cannot be discovered [23].

The other way is to let mass be the objective function and regard stiffness as a constraint condition. Ur-Rehman optimized mass of a 3-DoF PKM by setting ratio of force and deformation, i.e. stiffness value as constraint conditions [24]. Wu obtained geometric parameters of a 3-DoF PKM by taking mass and dexterity as objective functions, and strength as constraint condition. This constraint is calculated by stiffness matrix [25]. In such case, the allowed range of stiffness is pre-defined. The optimization turns into minimizing PKM mass while being subjected to specified stiffness ranges. This constraint transferring method cannot fully reflect the conflicting features between stiffness and mass of PKMs in the performance optimization.

Therefore, it is of vital importance to carry out the multi-objective optimization of PKM considering both stiffness and mass performances without any pre-defined preference. In addition, it is noted that the optimal parameters are directly applied to the construction of physical prototype after the optimization. In this process, parameters in the physical prototype cannot to be exactly the same as the optimized parameters due to the machining and manufacturing errors [26,27]. These parameter uncertainties would lead to the differences in the nominal and actual performances of PKMs. Although manufacturing and assembling errors can be minimized by accuracy improvement strategies, parameter uncertainty cannot be completely eliminated. In order to ensure the actual stiffness and mass performances are still be the same as the optimized results, the effect of parameter uncertainty should be addressed in the stiffness and mass optimization of PKMs.

Besides the consideration of multiple objectives and parameter uncertainty, the selection of optimization algorithm is also of vital importance. Traditional optimization algorithm uses local search procedure to search for the optimum. Convergent stepwise such as gradient, Hessian or linearity is applied. Such method heavily depends on good starting points. Global optima can only be found if the problem has certain convexity properties, or else it may fall into local optima [12]. To this end, global algorithm based on natural evolution has been introduced to the optimization of PKMs, for instance, genetic algorithm (GA) [16,28] and particle swarm optimization (PSO) [29–33]. In particular, PSO is a population-based stochastic optimization technique inspired by the social behavior of bird flocking or fish schooling. It has merits in terms of easy implementation and few parameters to adjust [34], thus is widely applied as optimization algorithm of PKMs. Yun [29] found that the fitness value of PSO is better than the traditional method in the optimal design of a 3-PUPU PKM. Shirazi [30] employed PSO to the optimization of a 6-DoF PKM. He indicated that fast convergence and easy variable constraining can be achieved by PSO. For the multi-objective optimization of a bio-inspired PKM, Zhang [31] used PSO to search for the overall optimal performance. The computing time was only 13.11 min. With similar manner, Wang [32] and Zhang [33] applied standard PSO to the optimal design of Tricept PKM and 3-DoF planar PKM. In their works, the efficiency of PSO was highly recognized. Overall, PSO has no evolutionary operators including crossover and mutation. It can be viewed as the extension and improvement of the working principle of GA. Therefore, PSO is selected as the optimization algorithm in our work.

Having outlined the state-of-art in Section 1, this paper is organized as follows. Formulation of stiffness and mass indices are carried out in Section 2, where the analytical mapping models between performance indices and design variables are established. Section 3 defines the constraint conditions by taking parameter uncertainty into account. The multi-objective optimization method is proposed and a cooperative equilibrium point is defined for obtaining the optimal result in Section 4. Taking a 5-DoF PKM as an example, Section 5 illustrates this stiffness and mass optimization approach before conclusions are drawn in Section 6.

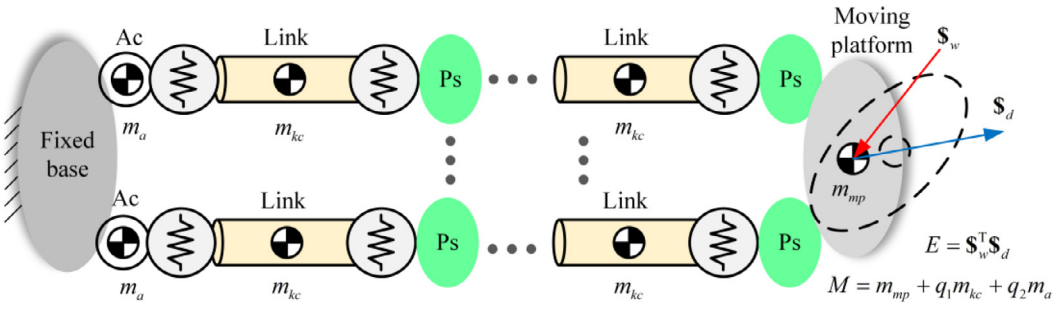

Fig. 1. Instantaneous energy and mass in motion of a general PKM.

2. Performance indices

2.1. Definition of stiffness and mass indices

The ultimate target for optimal design of PKM is to build a prototype that satisfies the end-user's requirements. The translation of end-user's requirements leads to performance indices that have clear physical meaning and are well-defined in the mathematical sense.

From viewpoint of physical meaning, stiffness is the measured ability that object resists deformations in response to applied external forces. Specially, the stiffness of a PKM under certain configuration within workspace can be characterized by its stiffness matrix. There have been intensive researches for defining stiffness index of PKM by the algebraic features of stiffness matrix, such as determinant [35], trace [36], eigenvalue and eigenvector [37,38]. But unit inconsistency of linear and angular stiffness makes these indices ambiguous in evaluating stiffness performance of PKMs. Alternately, instantaneous energy based stiffness indices [39] are adopted in this study.

According to Hooke's law, PKM with higher stiffness would generate smaller deformations when the same external payload is applied. Then instantaneous energy is converted from virtual work that is the product of instantaneous payload and deformations, as shown in Fig. 1. Therefore, smaller instantaneous energy indicates better stiffness performance of PKM.

Based on screw theory, instantaneous energy can be defined as

$$E = \mathbf{S}_w^T \mathbf{S}_d = \sum_{j_l=1}^{3} E_{j_l} + \sum_{j_a=1}^{3} E_{j_a},\ j_l = j_a = 1,2,3 \tag{1}$$

where E_{l,j_l} (E_{a,j_a}) represents the j_lth (j_ath) instantaneous energy. Instantaneous pure force $\mathbf{S}_{wl,j_l}$(moment $\mathbf{S}_{wa,j_a}$) does not do work on instantaneous angular deformation $\mathbf{S}_{da,j_a}$(deformation linear $\mathbf{S}_{dl,j_l}$), $E_{j_l} = |\mathbf{S}_{wl,j_l}^{\mathrm{T}} \mathbf{S}_{dl,j_l}|$, $E_{j_a} = |\mathbf{S}_{wa,j_a}^{\mathrm{T}} \mathbf{S}_{da,j_a}|$.

Instantaneous payload screw $\mathbf{S}_w$ can be expressed by the basis of the instantaneous payload screw subspace as

$$\mathbf{S}_w = \sum_{j_l=1}^{3} \rho_{l,j_l} \hat{\mathbf{S}}_{l,j_l} + \sum_{j_a=1}^{3} \rho_{a,j_a} \hat{\mathbf{S}}_{a,j_a},\ j_l = j_a = 1,2,3 \tag{2}$$

where $\hat{\mathbf{S}}_{l,i}$ and $\hat{\mathbf{S}}_{a,i}$ denote the base of instantaneous pure force and moment screw, ρ_{l,j_l} and ρ_{a,j_a} represent the magnitudes of $\mathbf{S}_{l,j_l}$ and $\mathbf{S}_{a,j_a}$, respectively. Moreover,

$$\hat{\mathbf{S}}_{l,i} = \begin{pmatrix} \boldsymbol{s}_i \\ \mathbf{0} \end{pmatrix},\ \hat{\mathbf{S}}_{a,i} = \begin{pmatrix} \mathbf{0} \\ \boldsymbol{s}_i \end{pmatrix},\ i = 1,2,3,\ \boldsymbol{s}_1 = \begin{pmatrix} 1 & 0 & 0 \end{pmatrix}^T,\ \boldsymbol{s}_2 = \begin{pmatrix} 0 & 1 & 0 \end{pmatrix}^T,\ \boldsymbol{s}_3 = \begin{pmatrix} 0 & 0 & 1 \end{pmatrix}^T \tag{3}$$

Assume $\boldsymbol{C}$ is the compliance matrix of PKM, $\hat{\mathbf{S}}_{c,i}$ is the eigenvector of the compliance matrix and $\lambda_{c,i}$ is the corresponding eigenvalue. It is noted that the dimension of the space spanned by instantaneous pure forces and moments is equal to the number of independent eigenvectors of compliance matrix. Then the base of the space $\hat{\mathbf{S}}_{l,i}$ and $\hat{\mathbf{S}}_{a,i}$ can be expressed by the linear combination of eigenvectors $\hat{\mathbf{S}}_{c,i}$ as follows

$$\hat{\mathbf{S}}_{l,j_l} = \sum_{i=1}^{6} \delta_{l,i,j_l} \hat{\mathbf{S}}_{c,i},\ \hat{\mathbf{S}}_{a,j_a} = \sum_{i=1}^{6} \delta_{a,i,j_a} \hat{\mathbf{S}}_{c,i},\ i = 1,2,\cdots 6 \tag{4}$$

where δ_{l,i,j_l} (δ_{a,i,j_a}) represents the linear coefficients of $\hat{\mathbf{S}}_{c,i}$. It can be calculated by

$$\begin{bmatrix} \delta_{l,1,j_l} & \delta_{l,2,j_l} & \cdots & \delta_{l,6,j_l} \end{bmatrix}^T = \boldsymbol{H}^{-1} \mathbf{S}_{l,j_l},\ \begin{bmatrix} \delta_{a,1,j_a} & \delta_{a,2,j_a} & \cdots & \delta_{a,6,j_a} \end{bmatrix}^T = \boldsymbol{H}^{-1} \mathbf{S}_{a,j_a}$$
$$\boldsymbol{H} = \begin{bmatrix} \hat{\mathbf{S}}_{c,1} & \hat{\mathbf{S}}_{c,2} & \cdots & \hat{\mathbf{S}}_{c,6} \end{bmatrix}$$

Substituting Eq. (4) into Eq. (2), leads to

$$\mathbf{\$}_w = \sum_{i=1}^{6}\left(\left(\sum_{j_l=1}^{3}\rho_{l,j_l}\delta_{l,i,j_l}\right)\hat{\mathbf{\$}}_{c,i}\right) + \sum_{i=1}^{6}\left(\left(\sum_{j_a=1}^{3}\rho_{a,j_a}\delta_{a,i,j_a}\right)\hat{\mathbf{\$}}_{c,i}\right) \tag{5}$$

In addition, instantaneous deformation screw $\mathbf{\$}_d$ can be calculated by Hooke's law as

$$\mathbf{\$}_d = \mathbf{C}\mathbf{\$}_w = \sum_{i=1}^{6}\left(\left(\sum_{j_l=1}^{3}\rho_{l,j_l}\delta_{l,i,j_l} + \sum_{j_a=1}^{3}\rho_{a,j_a}\delta_{a,i,j_a}\right)\lambda_{c,i}\hat{\mathbf{\$}}_{c,i}\right) \tag{6}$$

By substituting Eqs. (5) and (6) into Eq. (1), the instantaneous energy can be obtained as

$$E = E_l + E_a \tag{7}$$

$$E_l = \sum_{i=1}^{6}\left(\left(\sum_{j_l=1}^{3}\rho_{l,j_l}\delta_{l,i,j_l}\right)\left(\sum_{j_l=1}^{3}\rho_{l,j_l}\delta_{l,i,j_l} + \sum_{j_a=1}^{3}\rho_{a,j_a}\delta_{a,i,j_a}\right)\lambda_{c,i}\hat{\mathbf{\$}}_{c,i}^{T}\hat{\mathbf{\$}}_{c,i}\right) \tag{8}$$

$$E_a = \sum_{i=1}^{6}\left(\left(\sum_{j_a=1}^{3}\rho_{a,j_a}\delta_{a,i,j_a}\right)\left(\sum_{j_l=1}^{3}\rho_{l,j_l}\delta_{l,i,j_l} + \sum_{j_a=1}^{3}\rho_{a,j_a}\delta_{a,i,j_a}\right)\lambda_{c,i}\hat{\mathbf{\$}}_{c,i}^{T}\hat{\mathbf{\$}}_{c,i}\right) \tag{9}$$

Based on Eqs. (8) and (9), the instantaneous linear/angular stiffness performance index can be formulated by applying the instantaneous pure force/moment screw $\hat{\mathbf{\$}}_{l,i}/\hat{\mathbf{\$}}_{a,i}$ along/about x, y and z axis of the Cartesian coordinate as

$$\begin{cases}\eta_{l,x} = \left|\sum_{i=1}^{6}\left(\left(\rho_{l,1}\delta_{l,i,1}\right)^2\lambda_{c,i}\right)\right| \\ \eta_{l,y} = \left|\sum_{i=1}^{6}\left(\left(\rho_{l,2}\delta_{l,i,2}\right)^2\lambda_{c,i}\right)\right| \\ \eta_{l,z} = \left|\sum_{i=1}^{6}\left(\left(\rho_{l,3}\delta_{l,i,3}\right)^2\lambda_{c,i}\right)\right|\end{cases}, \quad \begin{cases}\eta_{a,x} = \left|\sum_{i=1}^{6}\left(\left(\rho_{a,1}\delta_{a,i,1}\right)^2\lambda_{c,i}\right)\right| \\ \eta_{a,y} = \left|\sum_{i=1}^{6}\left(\left(\rho_{a,2}\delta_{a,i,2}\right)^2\lambda_{c,i}\right)\right| \\ \eta_{a,z} = \left|\sum_{i=1}^{6}\left(\left(\rho_{a,3}\delta_{a,i,3}\right)^2\lambda_{c,i}\right)\right|\end{cases} \tag{10}$$

where η_{l,x_s}, η_{l,y_s} and η_{l,z_s} are defined as the instantaneous linear stiffness performance indices. Similarly, η_{a,x_s}, η_{a,y_s} and η_{a,z_s} are known as the instantaneous angular stiffness performance indices.

The local stiffness index of PKM can be further defined by

$$\eta = \left|\sum_{i=1}^{6}\left(\left(\sum_{j_l=1}^{3}\rho_{l,j_l}\delta_{l,i,j_l} + \sum_{j_a=1}^{3}\rho_{a,j_a}\delta_{a,i,j_a}\right)^2\lambda_{c,i}\right)\right| \tag{11}$$

where η is the overall stiffness index of PKM at a given point within workspace.

The global stiffness index of PKM is finally computed by evaluating stiffness performance all over the workspace as

$$\kappa_\eta = \frac{\int_V \eta dV}{V}\ ,\ \sigma_\eta = \frac{\sqrt{\int_V (\eta-\bar{\eta})^2 dV}}{V} \tag{12}$$

where V describes the volume of the workspace, $\bar{\eta}$ represents the mean value of η over the workspace.

It should be noted that the unit for instantaneous energy is always Joule no matter linear stiffness, angular stiffness or their combined effects are evaluated. The stiffness indices are invariant under a change of units. Therefore, the goal for best possible stiffness of PKM can be obtained by the global stiffness indices as

$$\kappa_\eta \to \min,\ \sigma_\eta \to \min \tag{13}$$

In addition, it might occur that some linear or angular stiffness is undesirable while the value of overall stiffness performance is desirable. This is called worst-case performance [40]. If end-user has requirement for stiffness along/about specific axis, the worst-case performance index needs to be concerned. It can be obtained by Eq. (10). Taking linear stiffness along x-axis as an example, the objective is formulated as

$$\eta_{l,x} \to \min \tag{14}$$

Mass in motion of PKM is the function of mechanism dimensions, i.e. link length, cross-section area, thickness. In general, mass in motion M is composed of the mass of moving platform m_{mp}, the mass of kinematic chains (intermediate links and joints) m_{kc} and the mass in motion of the actuators m_a (see Fig. 1). Thus,

$$M = m_{mp} + q_1 m_{kc} + q_2 m_a \tag{15}$$

where q_1, q_2 are the numbers of kinematic chains and actuators.

The mass of components can be easily calculated by using the geometry of the components and the density of their material. Consequently, the objective for mass performance is formulated as

$$M \to \min \tag{16}$$

2.2. Analytical mapping model between indices and parameters

After defining stiffness and mass indices, the mapping models between the indices and parameters of PKM needs to be built for the optimization. These mapping models are usually calculated by numerical analysis such as discrete searching strategy [11]. For the global stiffness indices κ_η and σ_η, the discrete searching strategy is implemented as follow.

Assume that the workspace is a regular geometry (cube, cylinder, etc.) in the 3-D space. This geometry is evenly meshed into finite elements. All the n_l nodes of these elements can be described by x, y, z-axis of Cartesian coordinates. Thus, the nodes represent different configurations of the PKM. Referring to Eq. (11), local stiffness η at each configuration can be calculated. κ_η and σ_η are determined by

$$\kappa_\eta = \frac{1}{n_l}\sum_{i=1}^{n_l}\eta_i,\ \ \sigma_\eta = \sqrt{\frac{1}{n_l}\sum_{i=1}^{n_l}\left(\eta_i - \kappa_\eta\right)} \tag{17}$$

It is noted that the accuracy of κ_η and σ_η depends on the n_l. The calculated κ_η and σ_η would greatly deviate from the true values if n_l is not big enough. This inaccuracy would be further accumulated in the optimization that searches for optimal result by iterative algorithm. In addition, exhaustive calculation at every node within workspace is repeated for each parameter set in the optimization process. The enormous iteration and high computational cost would lower the optimization efficiency.

Since the conventional numerical models have the problems of accuracy and efficiency, the way of establishing analytical mapping models is proposed in this study. A large n_l is set to calculate the stiffness and mass indices in a more accurate manner. Then the explicit and direct mathematical relationship between indices and parameters are built. By replacing the costly discrete searching, these mathematical relationships would reduce the calculation time thus improve optimization efficiency.

Dsign of experiment (DoE) and response surface method (RSM) [41] are employed to build the analytical mapping models. DoE carries out the calculation of performance indices under a set of parameters designed by statistical technique. On the basis of DoE, RSM explores the mathematical relationships by polynomial models. The establishment of the analytical mapping models is implemented as follows.

1) Determine different combinations of parameters by DoE. It can arrange moderate number of parameter sets that would provide enough information for the formulation of analytical mapping model.
2) Calculate performance indices by numerical models. For κ_η and σ_η, the numerical models are shown in Eq. (17). Herein, large value of n_l is given for improving the accuracy of calculated κ_η and σ_η.
3) Formulate the analytical mapping models by RSM. These analytical mapping models are expressed as polynomial surface functions, including linear, quadratic, cubic and quartic functions.
4) Select another m_l sets of parameters. Calculate the corresponding performance indices by numerical models and apply them to evaluate the accuracy of the analytical mapping models obtained in 3).

Mathematically, the linear, quadratic, cubic and quartic functions can be described as

$$\begin{aligned}
f_{\text{linear}}(\boldsymbol{x}) &= a_0 + \sum_{i=1}^{t} b_i x_i,\ \ f_{\text{quadratic}}(\boldsymbol{x}) = a_0 + \sum_{i=1}^{t} b_i x_i + \sum_{i=1}^{t} c_i x_i^2 + \sum_{i=1}^{t}\sum_{i<j}^{t} d_{ij} x_i x_j,\\
f_{\text{cubic}}(\boldsymbol{x}) &= a_0 + \sum_{i=1}^{t} b_i x_i + \sum_{i=1}^{t} c_i x_i^2 + \sum_{i=1}^{t}\sum_{i<j}^{t} d_{ij} x_i x_j + \sum_{i=1}^{t} e_i x_i^3,\\
f_{\text{quartic}}(\boldsymbol{x}) &= a_0 + \sum_{i=1}^{t} b_i x_i + \sum_{i=1}^{t} c_i x_i^2 + \sum_{i=1}^{t}\sum_{i<j}^{t} d_{ij} x_i x_j + \sum_{i=1}^{t} e_i x_i^3 + \sum_{i=1}^{t} f_i x_i^4
\end{aligned} \tag{18}$$

where $\boldsymbol{x}$ denote the parameters (design variables). a, b_i, c_i, d_{ij}, e_i and f_i are estimated regression coefficients obtained by least square method. $x_i x_j$ denotes interactions of any two parameters. x_i^2, x_i^3 and x_i^4 represent the second, third and fourth order nonlinearity.

For accuracy assessment of these polynomial surface functions, additional parameter sets are selected and the performance indices are calculated. Four metrics are applied to compute the errors between these calculated results and the polynomial functions. They are relative average absolute error (RAAE), relative maximum absolute error (RMAE), root mean

square error (RMSE) and R square (R^2) [42].

$$\mathrm{RAAE} = \frac{\sum_{q=1}^{m_l} \left|y_q - \hat{y}_q\right|}{\sum_{q=1}^{m_l} |y_q - \bar{y}|},\ \mathrm{RMAE} = \frac{\max\left\{\left|y_q - \hat{y}_1\right|, \cdots, \left|y_q - \hat{y}_{m_l}\right|\right\}}{\sum_{q=1}^{m_l} |y_q - \bar{y}|/m_l},$$
$$\mathrm{RMSE} = \sqrt{\frac{\sum_{q=1}^{m_l} (y_q - \bar{y})^2}{m_l}},\ \mathrm{R}^2 = 1 - \frac{\sum_{q=1}^{m_l} \left(y_q - \hat{y}_q\right)^2}{\sum_{q=1}^{m_l} (y_q - \bar{y})^2} \tag{19}$$

where y_q denote the exact value at evaluation parameter set q, $\hat{y}_q$ is the calculated value by the surface function, $\bar{y}$ is the mean value of y_q, m_l is the number of additional evaluation parameter sets.

In general, a large value of R^2 and small values of RAAE, RMSE are preferred. They indicate that the analytical model has high accuracy in the overall design space. But the analytical model can be less accurate in some region although good global measurements are given by R^2, RAAE and RMAE. Thus, a smaller RMSE is necessary for focusing on the maximum error in one region. With the consideration of both global accuracy and maximum error from the four matrices, the appropriate analytical model with high accuracy can be achieved. By applying these analytical models, the efficiency of the optimization will be greatly improved.

3. Constraint condition based on parameter uncertainty

Constraint conditions for stiffness and mass optimization of PKM can be classified into geometric and performance constraints, such as stroke of prismatic joint and minimal linear stiffness along specific axis. They come from geometric features of PKM or the end-user's requirements. In the conventional optimization, nominal values of parameters are applied to calculate if the constraint conditions are satisfied. Optimal parameters are determined from those who do not violate the constraint conditions. Finally the physical prototype of PKM is built by directly applying these optimal parameters.

However, the actual parameters of physical prototype can hardly be the same as the nominal parameters. These differences in parameters are mainly caused by machining and assembling errors during construction. The constraint conditions might be violated under the actual parameters, leading to the failure of applying optimization results. Since the manufacturing errors cannot be completely eliminated, difference between nominal and actual parameters always exist and their effects should be addressed during the optimization.

PKM parameters can be regarded as uncertain design variables. For example, in the manufacturing or construction of the physical prototype, parameters are specified by tolerance as $x \pm \Delta x$, where x is the nominal value and Δx is the tolerance. It indicates that any value within the range $[x - \Delta x, x + \Delta x]$ is acceptable for the physical prototype. This randomness makes it difficult to model the parameter uncertainties and access their effects in an explicit manner.

Probabilistic simulation method is applied to formulate the parameter uncertainty model in this paper. Assume that $\boldsymbol{x} = \{x_1, x_2, \cdots, x_n\}^{\mathrm{T}}$ denote the design variables of the PKM. For each design variable x_i $(i = 1, 2, \cdots, n)$, N random values can be generated by specifying its mean value $\bar{x}_i$ and standard deviation σ_{x_i}. Herein, mean value $\bar{x}_i$ is assigned as its nominal value and standard deviation σ_{x_i} is determined by parameter tolerance. These N random samples are assumed to be subjected to normal distribution. This is because the manufacturing errors usually follow normal distribution. It is to be noted that any non-normal distribution of the parameter uncertainty can be replaced by an equivalent normal distribution using Rosenblatt transformation. Thus, the design variable $\boldsymbol{x}$ become

$$\boldsymbol{X} = \left\{\boldsymbol{X}_1, \boldsymbol{X}_2, \cdots, \boldsymbol{X}_j, \cdots, \boldsymbol{X}_N\right\},\ j = 1, 2, \cdots, N \tag{20}$$

$$\boldsymbol{X}_j = \left\{x_{1,j}, x_{2,j}, \cdots, x_{i,j}, \cdots, x_{n,j}\right\},\ i = 1, 2, \cdots, n \tag{21}$$

where $\boldsymbol{X}$ is the model of design variables with parameter uncertainties, $\boldsymbol{X}_j$ denotes the jth set of random design variables, $x_{i,j}$ represents the jth random value for design variable x_i.

Therefore, design variable with parameter uncertainty can be described by $\boldsymbol{X}$ after determining $\bar{x}_i$, σ_{x_i} and N by probabilistic simulation method. Then probabilistic constraints are defined to evaluate the effects of parameter uncertainty during optimization.

The conventional constraint conditions with nominal parameters can be expressed by

$$\begin{cases} g(\boldsymbol{x}) \geq 0 \\ g(\boldsymbol{x}) = g_{\mathrm{r}}(\boldsymbol{x}) - g_{\mathrm{c}}^{\mathrm{L}} \mathrm{or} g(\boldsymbol{x}) = g_{\mathrm{c}}^{\mathrm{U}} - g_{\mathrm{r}}(\boldsymbol{x}) \end{cases} \tag{22}$$

where $g_{\mathrm{c}}^{\mathrm{U}}$, $g_{\mathrm{c}}^{\mathrm{L}}$ are the upper and lower limits of constraint condition, $g_{\mathrm{r}}(\boldsymbol{x})$ is the response corresponding to $\boldsymbol{x}$. For example, the lower limit of linear stiffness along x-axis is given as 2 N/μm by end-user. Under certain $\boldsymbol{x}$, $g_{\mathrm{r}}(\boldsymbol{x})$ is calculated as 1.98 N/μm. Then the constraints is violated since $g(\boldsymbol{x}) = 1.98 - 2 < 0$.

In order to unify the units of the constraints, constraint conditions can be reformulated as

$$\begin{cases} s(\boldsymbol{x}) \geq 1 \\ s(\boldsymbol{x}) = \frac{g_c^U}{g_r(\boldsymbol{x})} \text{or} s(\boldsymbol{x}) = \frac{g_r(\boldsymbol{x})}{g_c^L} \end{cases} \tag{23}$$

where $s(\boldsymbol{x})$ is defined as safety factor. It is the measured factor for describing the safety of the optimization under certain design variables.

Based on Eqs. (20)–(23), the constraints with the consideration of parameter uncertainty are defined by probabilistic method as

$$P(s(\boldsymbol{X}) \geq 1) \geq P_p \tag{24}$$

where $P(s(\boldsymbol{X}) \geq 1)$ denotes the probability that optimization constraints are satisfied. $P_p \in (0, 1)$ is a pre-defined probability given by end-user.

For the design variables with parameter uncertainty $\boldsymbol{X}$, their safety factors $s(\boldsymbol{X})$ are firstly calculated to evaluate whether they satisfy the constraints. Then the probability of $s(\boldsymbol{X}) \geq 1$ is computed. If this probability is greater than P_p, it indicates that parameter uncertainty won't have much influence on the optimization results. If not, the physical prototype built by nominal parameters would be affected by parameter uncertainty.

For the sake of simplifying Eq. (24), a probabilistic sufficiency factor P_{sf} is proposed. It is defined as the solution to following equation

$$P(s(\boldsymbol{X}) \geq P_{\text{sf}}) = P_p \tag{25}$$

where P_{sf} is the safety factor that is violated with the required probability P_p. Rank the safety factors $s(\boldsymbol{X})$ in ascending order as $\{s_1, s_2, \cdots, s_N\}$, $s_i < s_{i+1}$, $i = 1, 2, \cdots, N$. Then P_{sf} can be determined from

$$P_{\text{sf}} = s_r, \ N(1 - P_p) - 1 < r \leq N(1 - P_p) \tag{26}$$

A P_{sf} of 1.0 implies that the probability of $s(\boldsymbol{X}) \geq 1$ is equal to the target value P_p, a P_{sf} larger than one means that the probability of $s(\boldsymbol{X}) \geq 1$ exceed the target, and a P_{sf} less than one means that the PKM is not as safe as the end-user's requirements. Therefore, $P_{\text{sf}} \geq 1$ has the same physical meaning as Eq. (24). The probabilistic constraints in the optimization of PKMs can be expressed as

$$P_{\text{sf},k} \geq 1, \ k = 1, 2, \cdots, q \tag{27}$$

where q denotes total number of constraints.

4. Stiffness and mass optimization method

4.1. Particle swarm optimization algorithm

PSO is initialized with a population of random solutions and search for optima by updating generations. The population and individual are called swarm and particles respectively. Each particle moves with an adaptable velocity and keeps a memory for the best position it has ever found. Then the best solution encountered by all the particles is compared and selected. Every particle modifies its direction towards its best position and the global position, which will provide convergence in searching [43]. The process for implementing PSO is described as

1) Initialization. A population of particles with positions and velocities are randomly generated in the search space. The current position of each particle is set as p_i, and the best fitness value of current population is given by p_g.
2) Comparison and selection. Each particle is evaluated by the fitness function. The fitness value of the particle is compared with p_i. If the fitness value is better than p_i, then let p_i equal to this value. Then, the fitness value of the particle is compared with p_g. If the value is better than p_g, then reset p_g to the current particle's position and value.
3) Adjustment. The position q_i and velocity v_i of each particle is changed by the following equations

$$\begin{cases} q_i(t+1) = q_i(t) + v_i(t+1) \\ v_i(t+1) = wv_i(t) + R_1\varsigma_1(p_i - q_i(t)) + R_2\varsigma_2(p_g - q_i(t)) \end{cases} \tag{28}$$

where w is the inertia weight, R_1 and R_2 are two distinct random values distributed between 0 and 1, ς_1 and ς_2 are the acceleration constants known as personal and global learning coefficients.

4) Check if termination criterion is met, usually the termination criterion is the sufficient fitness or maximum number of iterations. If yes, then stop searching. If no, loop to step 2).

Having proved the effectiveness and efficiency in solving optimization problems, PSO is adopted in the stiffness and mass optimization of PKMs with the aid of software, such as Matlab (MathWork), Isight (Dassault Systemes).

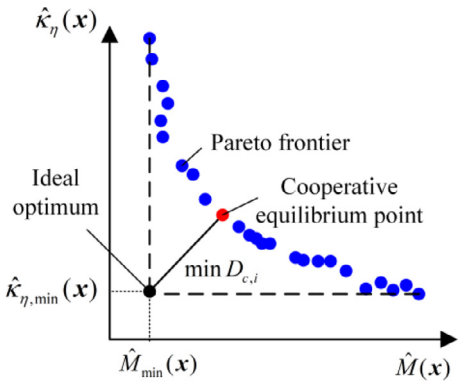

Fig. 2. Cooperative equilibrium point for the two-objective optimization.

4.2. Cooperative equilibrium point

The multi-objective optimization is applied to deal with the stiffness and mass optimization of PKM. The target is to find the best design variables of the PKM that have simultaneously the smallest instantaneous energy and mass in motion. It can be described in mathematical terms as follows.

$$\begin{cases} \min F(\boldsymbol{x}) = \{f_1(\boldsymbol{x}), f_2(\boldsymbol{x}), \cdots, f_l(\boldsymbol{x})\} \\ s.t\ P_{\mathrm{sf},k}(\boldsymbol{x}) \geq 1, k = 1, 2, \cdots, q \\ \boldsymbol{x}^{\mathrm{L}} \leq \boldsymbol{x} \leq \boldsymbol{x}^{\mathrm{U}} \end{cases} \tag{29}$$

where $f_1(\boldsymbol{x}), f_2(\boldsymbol{x}), \cdots, f_l(\boldsymbol{x})$ are the stiffness and mass objective functions, $P_{\mathrm{sf},k}(\boldsymbol{x})$ is the probabilistic constraints considering parameter uncertainty, $\boldsymbol{x}^{\mathrm{U}}$ and $\boldsymbol{x}^{\mathrm{L}}$ are upper and lower limits of parameters.

By simultaneously optimizing the stiffness and mass objective functions without any pre-defined relations, not a particular solution, but a cluster of solutions are obtained. The image of all these solutions is called Pareto frontier. It indicates that none of the objective functions can be further increased without a decrease of some of remaining objective functions. Pareto frontier shows the compromise among multiple objective functions. Usually the final solution is left to the end-users. One may choose the point that has smaller mass while another one prefers the point with higher stiffness according to different applications of PKM. Herein, a cooperative equilibrium searching method is proposed to find the best compromise among multiple objective functions when they are assumed to be equally important.

Exampled by two-objective optimization in terms of global stiffness index κ_η and mass in motion M, the cooperative equilibrium searching method is illustrated. If the two objective functions are assumed to correspond to two players, the process to determine the final solution from Pareto frontier can be regarded as a cooperative game. In the game, each player tries to find his maximum possible benefit considering the shared information from the other player. The ideal solution is the one that both players get their best interests. But it cannot be reached as shown in the Pareto frontier in Fig. 2. The cooperation between players can be assessed by the gap between existing solutions and the ideal solution. The solution that is the closet to the ideal point is defined as the cooperative equilibrium point, which is selected as the final solution.

Mathematically, the cooperative game is played as follows. Dimensionless processing is firstly made to the points on Pareto frontier.

$$\hat{\kappa}_{\eta,i}(\boldsymbol{x}) = \frac{\kappa_{\eta,i}(\boldsymbol{x}) - \bar{\kappa}_{\eta,i}(\boldsymbol{x})}{\tilde{\kappa}_{\eta,i}(\boldsymbol{x})},\ \hat{M}_i(\boldsymbol{x}) = \frac{M_i(\boldsymbol{x}) - \bar{M}(\boldsymbol{x})}{\tilde{M}(\boldsymbol{x})} \tag{30}$$

where $\bar{\eta}_{K,i}(\boldsymbol{x})$, $\bar{M}(\boldsymbol{x})$ are the mean values for κ_η and M on Pareto frontier, $\tilde{\eta}_{K,i}(\boldsymbol{x})$, $\tilde{M}(\boldsymbol{x})$ are corresponding standard deviation.

Then, the best value of each objective is found on the Pareto frontier. Ideal optimum is formed by these best values. Distances from Pareto points to this ideal point can be computed as

$$D_{c,i} = \sqrt{\left(\hat{\kappa}_{\eta,i}(\boldsymbol{x}) - \hat{\kappa}_{\eta,\min}(\boldsymbol{x})\right)^2 + \left(\hat{M}_i(\boldsymbol{x}) - \hat{M}_{\min}(\boldsymbol{x})\right)^2} \tag{31}$$

where $\hat{\kappa}_{\eta,\min}(\boldsymbol{x})$, $\hat{M}_{\min}(\boldsymbol{x})$ is the minimal stiffness index and minimal mass on the Pareto frontier.

Therefore, the cooperative equilibrium point is determined as the Pareto point with minimum $D_{c,i}$. When there are h objective functions, the cooperative equilibrium point can be further determined by

$$D_{c,i} = \sqrt{\sum_{i=1}^{h} \left(f_{c,i}(\boldsymbol{x}) - f_{i,\min}(\boldsymbol{x})\right)^2} \tag{32}$$

where $f_{c,i}(\boldsymbol{x})$ is the value of ith objective for cth Pareto point. $f_{i,\min}(\boldsymbol{x})$ is the minimum value of ith objective.

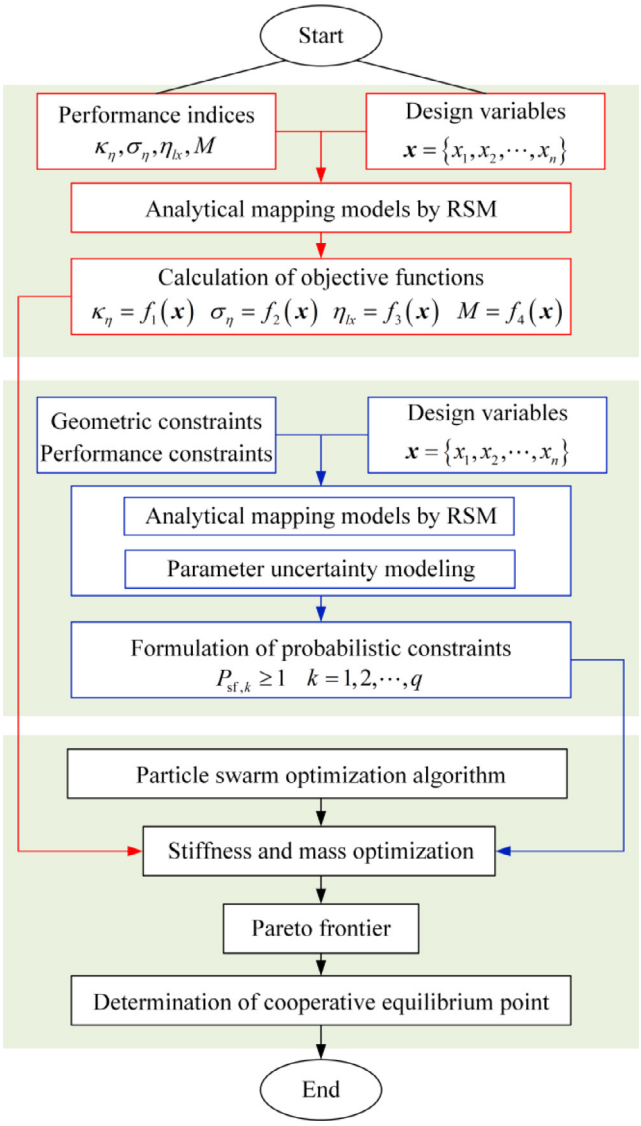

Fig. 3. Procedure for stiffness and mass optimization of PKM.

4.3. Summary of the optimization procedure

The proposed methodology for stiffness and mass optimization of PKM is summarized in Fig. 3. It can roughly be divided into three steps as follows.

Step 1) stiffness and mass indices are calculated.

Referring to Eqs. (10) and (12), both the overall stiffness performance within workspace and the worst-case performance are considered (For the PKM with horizontal layout, the worst-case performance is considered as linear stiffness along gravitational direction). Masses of moving parts are added to formulate mass index by Eq. (15). For the sake of ensuring accuracy and efficiency of the optimization, analytical mapping models of performance indices and design variables are established by RSM. The polynomial functions shown in Eq. (18) are obtained and the accuracy assessments are implemented. The analytical mapping model with the highest accuracy are selected as the objective functions.

Step 2) constraint conditions are formulated.

Geometric constraints (interference among limbs, rotational angles of joints, etc.) and performance requirements (allowable elastic deformations, stiffness along each direction, etc.) are translated from the end-user's requirements. The response of the constraints $g_{r,k}(\boldsymbol{x})$ $(k = 1, 2, \cdots, q)$ is calculated by numerical analysis. Then $g_{r,k}(\boldsymbol{x})$ and design variables are characterized by analytical mapping models built by RSM. On this basis, N random samples are generated to simulate the parameter uncertainties. And the probabilistic sufficiency factors $P_{sf,k}$ $(k = 1, 2, \cdots, q)$ is calculated by Eq. (26). Applying RSM again,

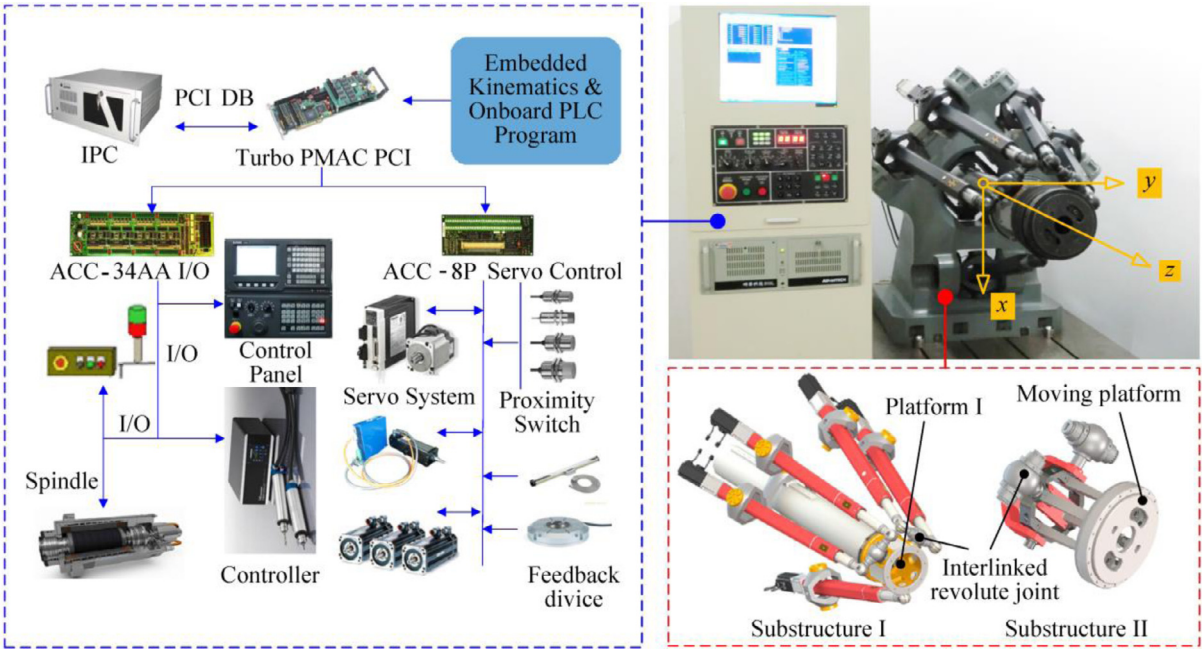

Fig. 4. Prototype of T5 PKM and its control system.

Table 1
Workspace and design constraints of T5 PKM.

Work envelope			Allowable capability				
R	h	$\varphi_{\max}$	t_m	$k_{lx,\min}$	$k_{ly,\min}$	$k_{lz,\min}$	$k_{\alpha z,\min}$
mm	mm	deg	mm	N/um	N/um	N/um	N · m/rad
300	200	30	4	3	3	10	1×10^6

the analytical mapping models of $P_{\mathrm{sf},k}$ and design variables are established. The constraint conditions considering parameter uncertainty are formulated by Eq. (27).

Step 3) the multi-objective optimization is implemented with the aid of PSO.

Pareto frontier is obtained after simultaneously optimizing stiffness and mass indices without pre-defined preferences. Finally, the cooperative equilibrium point is determined by Eqs. (30) and (32).

5. Case study

A 5-DoF PKM (named as 'T5 PKM') is introduced to demonstrate the proposed mass and stiffness optimization method. The T5 PKM consists of substructure I and substructure II articulated by interlinked revolute joints [44]. Substructure I is composed of fixed base, five UPS limbs, one UP limb and platform I. It has 3-DoF motion capabilities. Two redundant limbs provide extra supports to platform I thus enhance stiffness performance of substructure I. Substructure II consists of two closed-loops connected by a R joint. The closed-loops are with parallelogram structure whose topology is RUUR. It is capable of 2-DoF rotations. Instead of embedding servo motors, actuations of substructure II are from the redundant motions of substructure I. Hence, the weight of rotating head is reduced. In addition, high stiffness of substructure II can be achieved on account of the parallelogram structure and over-constrained feature [45].

Prototype of T5 PKM is illustrated in Fig. 4. The fixed base and platform I are made of cast iron. The limbs, interlinked revolute joint, parallel structures and moving platform are manufactured with steel. The current version of T5 PKM is configured with a cylindrical workspace whose radius (R) is 300 mm and height (H) is 200 mm (see Table 1). The rotating capability of structure II about A/B axis ($\varphi_{\max}$) is $\pm 30^\circ$. Industrial personal computer (IPC) and programmable multi axes controller (PMAC) are applied to establish control system. Control command can be given by manual programming or graphic interface.

Geometric and engineering constraints are listed in Table 1. Since the limbs are designed as tubes, the minimal thickness (t_m) of these tubes is given. Lower limit of linear stiffness along each direction ($k_{lx,\min}$, $k_{ly,\min}$, $k_{lz,\min}$), angular stiffness about z-axis ($k_{\alpha z,\min}$) are set. Parameters and corresponding ranges are shown in Table 2. Sectional parameters and stiffness coefficients of substructure I are listed in the first row. Diameter of interlinked revolute joint, sectional parameters and compliance coefficients are shown in the second row (detail explanation of these parameters refer to [46]). Thus, stiffness

Table 2
Design parameters and their ranges.

D_{op}(mm) [68,80]	d_s(mm) [18,28]	D_{ip}(mm) [45,58]	k_s(N/μm) [400,800]	D_{ct}(mm) [153,187]	d_{ct}(mm) [150,170]	d_{s5}(mm) [18,30]	k_{s5}(N/μm) [600,900]
d_{ir2}(mm) [40,65]	a_{11}(mm) [10,18]	a_{21}(mm) [20,30]	b_{12}(mm) [20,38]	c_{11}(μm/N) [3×10^{-4},6×10^{-4}]	c_{21}(μm/N) [1×10^{-3},3×10^{-3}]	c_{31}(μm/N) [6×10^{-5},9×10^{-5}]	

Table 3
Accuracy assessment for analytical mapping models of objectives.

Order		M	κ_η	σ_η	η_{lx}
R^2	1	0.9995	0.9054	0.8366	0.9044
	2	1	0.9940	0.9806	0.9924
	3	1	0.9998	0.9957	0.9992
	4	1	0.9999	0.9992	0.9997
RAAE	1	0.0047	0.0557	0.0745	0.0688
	2	2.6399×10^{-8}	0.0146	0.0243	0.0201
	3	3.0355×10^{-8}	0.0031	0.0114	0.0059
	4	2.8848×10^{-8}	0.0007	0.0057	0.0034
RMAE	1	0.0015	0.18199	0.3693	0.2071
	2	8.4417×10^{-8}	0.04790	0.0835	0.0784
	3	8.8193×10^{-8}	0.00874	0.0794	0.0220
	4	8.8370×10^{-8}	0.00325	0.0215	0.0136
RMSE	1	0.0057	0.06715	0.0943	0.0827
	2	3.2246×10^{-8}	0.01832	0.0297	0.0248
	3	3.6331×10^{-8}	0.00372	0.0160	0.0074
	4	3.5141×10^{-8}	0.0009	0.0072	0.0044

and mass matching design of T5 PKM is expressed as

$$\begin{cases} \min F(\boldsymbol{x}) = \{\kappa_\eta, \sigma_\eta, \eta_{lx}, M\} \\ s.t\ P_{\mathrm{sf},k} \geq 1, k = 1,2,3,4 \\ T(\boldsymbol{x}) \geq 0 \\ \boldsymbol{x}^{\mathrm{L}} \leq \boldsymbol{x} \leq \boldsymbol{x}^{\mathrm{U}} \end{cases} \tag{33}$$

where $T(\boldsymbol{x})$ is the geometric constraints, including interference among limbs, stroke of prismatic joints, rotational ranges of joints and thickness of the tubes.

Following the optimization procedure proposed in Section 4, the stiffness and mass optimization of T5 PKM is implemented as follows.

Step 1) Calculation of stiffness and mass indices

Analytical mapping models of the performance indices are firstly established. DoE is employed to determine numbers and of parameter sets. Numbers of parameter sets are determined by the numbers of coefficients in analytical mapping model. It has been reported that at least twice more than model coefficients are recommended [27]. Herein, there are 15 parameters in the stiffness and mass optimization of T5 PKM (see Table 2). It is known from Eq. (18) that quartic function has the most coefficients (166 coefficients for T5 PKM). Thus, 332 sets of parameters are generated by DoE. Resorting to the numerical analysis, values of performance indices correspond to these parameters are calculated. Then, RSM is employed to formulated the linear, quadratic, cubic and quartic functions. Additional 50 random sets of parameters are generated for the accuracy assessments of these analytical functions. The four metrics are calculated by Eq. (19), and the results are listed in Table 3. The analytical function with highest R^2 and smallest RAAE, RMAE and RMSE should be selected. Therefore, quadratic and quartic functions are determined as the analytical mapping models for mass and all the stiffness performances (gray area in Table 3).

Step 2) Formulation of constraint conditions

Parameter uncertainty is considered in the formulation of constraints. In order to evaluate the effects of the parameter uncertainty to the performance constraints in an efficient manner, analytical mapping models for the response of constraints (k_{lx}, k_{ly}, k_{lz}, $k_{\alpha z}$) are established. With a similar way to the objective functions, 332 sets of parameters are generated by DoE. RSM is applied and the accuracy assessments are shown in Table 4. It is found that cubic model is suitable for k_{ly} while quartic models are considered for the rest constraints.

N random samples are generated for each parameter by specifying mean value and variation. Herein, N is set to be 10,000 for better estimation of parameter uncertainty. Mean value is given by the nominal value of parameters. Coefficient of variation (CoV) of sectional parameters is given as 0.01. And CoV of stiffness/compliance coefficients is assigned as 0.0025. Thus, parameter uncertainty model is built. Based on the analytical models of k_{lx}, k_{ly}, k_{lz}, $k_{\alpha z}$, safety factors of the parameter uncertainty model can be easily calculated by Eq. (23). Assume that parameter uncertainty would have little influence on the physical prototype if 95% of the safety factors satisfy the constraints ($s(\boldsymbol{X}) \geq 1$). Hence, $P_p = 0.95$. With $P_p$and the N safety factors, P_{sf} can be computed by Eq. (26). On this basis, probabilistic constraints shown in Eq. (27) can be formulated.

Table 4
Accuracy assessment for analytical mapping models of performance constraints.

Order		k_{lx}	k_{ly}	k_{lz}	$k_{\alpha z}$
R^2	1	0.9260	0.8921	0.9356	0.9694
	2	0.9839	0.9225	0.9964	0.9995
	3	0.9862	0.9943	0.9998	0.9999
	4	0.9889	0.9607	0.9998	0.9999
RAAE	1	0.0603	0.0634	0.0533	0.0429
	2	0.0258	0.0744	0.0136	0.0054
	3	0.0233	0.0765	0.0028	0.0009
	4	0.0224	0.0751	0.0025	0.0008
RMAE	1	0.1729	0.4162	0.1713	0.1400
	2	0.1188	0.2428	0.0369	0.0168
	3	0.1357	0.1119	0.0146	0.0032
	4	0.1252	0.1387	0.0161	0.0032
RMSE	1	0.0721	0.0934	0.0629	0.0505
	2	0.0346	0.1154	0.0159	0.0066
	3	0.0321	0.1094	0.0037	0.0011
	4	0.0304	0.1157	0.0034	0.0010

Table 5
Accuracy assessment for analytical mapping models of probabilistic sufficiency factors.

Order		$P_{sf,1}$	$P_{sf,2}$	$P_{sf,3}$	$P_{sf,4}$
R^2	1	0.9087	0.7162	0.9354	0.9674
	2	0.9933	0.8584	0.9959	0.9995
	3	0.9975	1	0.9995	1
	4	1	1	1	1
RAAE	1	0.0539	0.0826	0.0541	0.0434
	2	0.0146	0.0653	0.0102	0.0053
	3	0.0098	0.0002	0.0014	0.0003
	4	0.0000	0.0001	0.0000	0.0000
RMAE	1	0.2187	0.2486	0.16536	0.13187
	2	0.0690	0.2395	0.03161	0.02257
	3	0.0281	0.0006	0.00477	0.00128
	4	0.0003	0.0005	0.0000	0.0000
RMSE	1	0.0683	0.1010	0.0666	0.0523
	2	0.0190	0.0825	0.0126	0.0067
	3	0.0124	0.0002	0.0018	0.0004
	4	0.0000	0.0002	0.0000	0.0000

Table 6
Settings of multi-objective particle swarm optimization.

Parameter	Setting
Maximum iterations	100
Number of particles	100
Inertia weight (w)	0.729
Global learning coefficient (ς_1)	1.49
Personal learning coefficient (ς_2)	1.49

For the convenience of calculating P_{sf}, analytical mapping models between P_{sf} and the parameters are investigated. RSM is applied again to formulate analytical functions of $P_{sf,k}$ $(k = 1, 2, 3, 4)$. Accuracy assessment is carried out and the results are listed in Table 5. It shows that quartic functions should be chosen.

Step 3) Determination of cooperative equilibrium point

After formulating analytical mapping models of objectives and probabilistic constraints, PSO is applied to solve the stiffness and mass optimization with the aid of Matlab and Isight software. The setting of PSO is shown in Table 6. For the sake of convergence of the algorithm, initial weight w is set as 0.729 while ς_1 and ς_2 are given as 1.49. Optimization results are shown in Figs. 5 and 6. There are 1029 feasible solutions that satisfy the probabilistic constraints. Parameter values of the feasible points are shown from Fig. 5a to c. From the feasible points, 256 points are flagged as Pareto frontier. These Pareto points are selected from the sum of objectives and penalty that are among 150 to 300. Parameter values of the Pareto points are shown in the parallel coordinate chart in Fig. 5e. It indicates from the parameter values that larger d_{ir2}, a_{11}, b_{12} are required to form Pareto frontier.

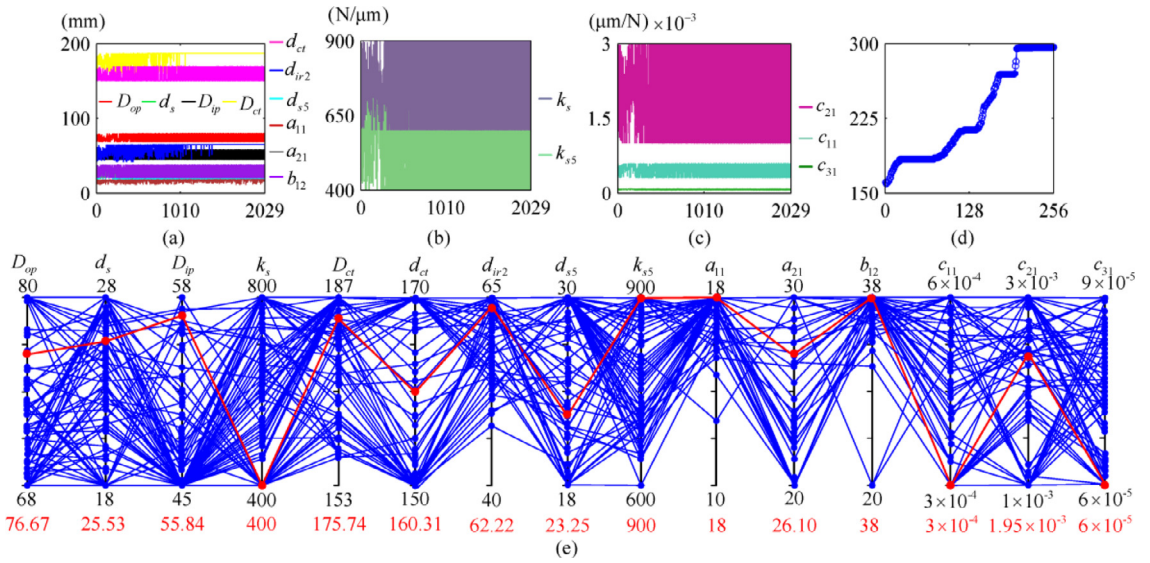

Fig. 5. (a) Sectional parameters of feasible points, (b) Stiffness coefficients of feasible points, (c) Compliance coefficients of feasible points, (d) Objectives and penalty of Pareto points, (e) Parameters of Pareto points.

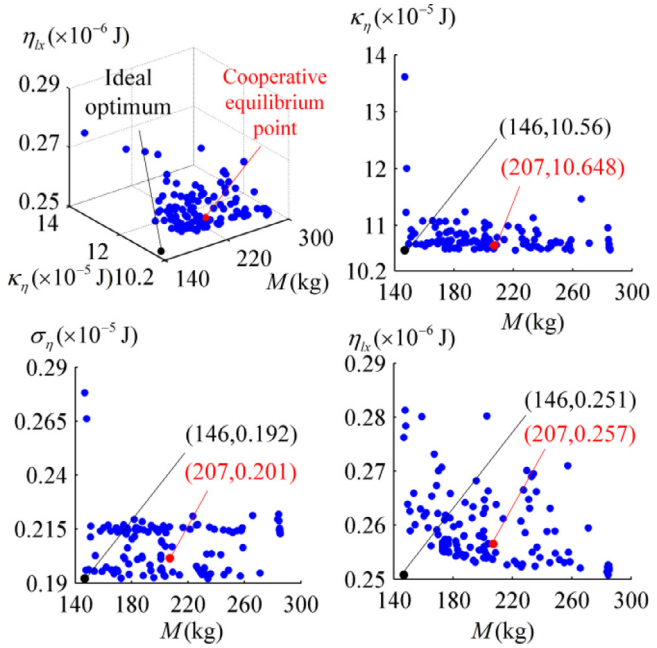

Fig. 6. Pareto frontier of the stiffness and mass optimization of T5 PKM.

Pareto frontier for the stiffness and mass optimization of T5 PKM is shown in Fig. 6. Minimal values of M, κ_η, σ_η and η_{lx} are obtained from the Pareto frontier. They are 146.7251 kg, 10.5641×10^{-5}J, 0.1921×10^{-5}J and 0.2508×10^{-6}J, respectively. Ideal optimum is formed by these individual minimums. Dimensionless method is then applied to the objectives on Pareto frontier by Eq. (30). Then distance from Pareto points to the ideal optimum are calculated by Eq. (32). The cooperative equilibrium point is determined as the Pareto point with minimal distance to the ideal point. The values of M, κ_η, σ_η and η_{lx} at cooperative equilibrium point are 207.1056 kg, 10.648×10^{-5}J, 0.2015×10^{-5}J and 0.2565×10^{-6}J.

Optimal parameters corresponding to the cooperative equilibrium point are demonstrated by the red lines in Fig. 5e. Virtual prototype is built according to these parameters. The mass of T5 PKM increases 17.17% after optimization. The detail process for the calculation of stiffness of T5 PKM is referred to [45]. The position of end-reference point is denoted by (x, y, z). Herein, the plane $z = 1200$ mm is selected.

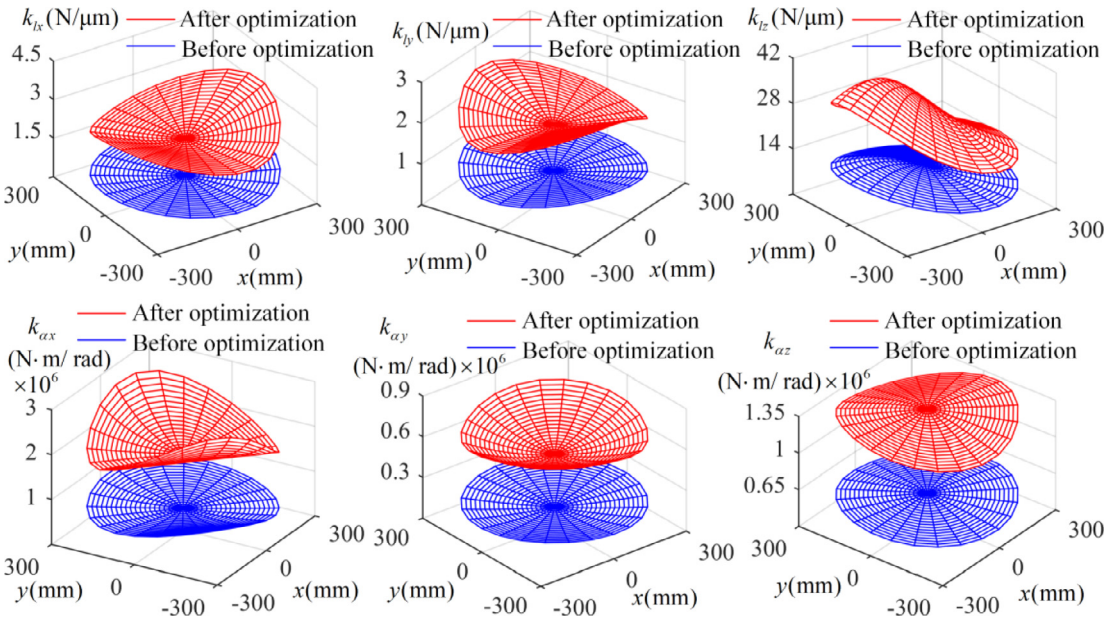

Fig. 7. Stiffness distribution of T5 PKM before and after optimization.

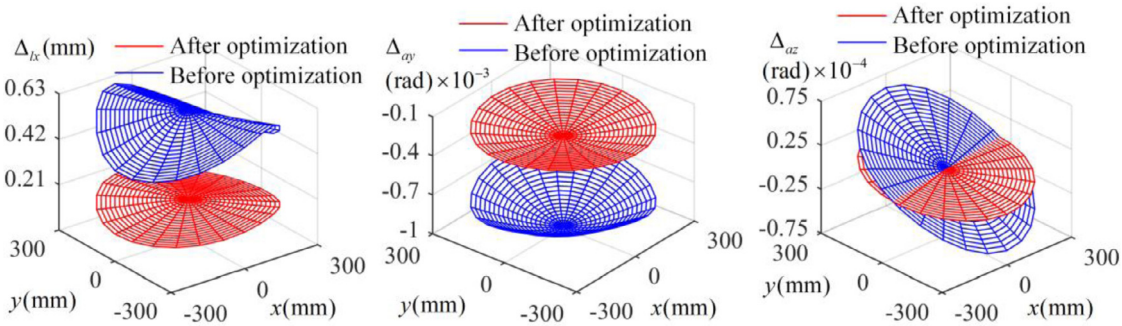

Fig. 8. Deformations caused by gravity of T5 PKM before and after optimization.

Distributions of linear and angular stiffness of T5 PKM within workspace are demonstrated in Fig. 7. It is found out that: (1) Linear stiffness k_{lx}, k_{ly} and k_{lz} are all plane-symmetrical before and after optimization. (2) Linear stiffness k_{lx} and k_{ly} are symmetrical about plane $y = 0$ and $x = 0$. The value of k_{lx} and k_{ly} are minimal near symmetrical plane (0.5637 N/μm and 0.5321 N/μm before optimization, 1.6686 N/μm and 1.7103 N/μm after optimization). k_{lx} and k_{ly} are getting larger when the end reference point is closing to the workspace boundary. (3) Distribution of k_{lz} is symmetrical about plane $y = 0$. Before optimization, the maximum k_{lz} is 14.6172 N/μm. And it becomes 45.6057 N/μm after optimization. The values of k_{lz} are much larger than those of k_{lx} and k_{ly}. (4) Distribution of $k_{\alpha x}$, $k_{\alpha y}$ and $k_{\alpha z}$ are symmetrical about plane $y = -x$ before and after optimization. Variation of $k_{\alpha x}$ and $k_{\alpha y}$ are contrary to that of $k_{\alpha z}$. (5) the minimum $k_{\alpha x}$, $k_{\alpha y}$ and $k_{\alpha z}$ before optimization are 0.4694, 0.3969 and 0.5387 $\times 10^6$N · m/rad. They become 1.5209, 1.1590 and 1.8855 $\times 10^6$N · m/rad after optimization.

On the whole, changing tendency of linear and angular stiffness of T5 PKM are similar before and after optimization. In addition stiffness after optimization is nearly 3 times larger than that before optimization.

The visual and direct impact of mass to the PKM performance is the deformation of PKM resulted from its gravity. For the sake of efficient assessment, equivalent gravity of T5 PKM is considered [45]. It mainly leads to linear deformation along x-axis Δ_{lx}, angular deformation about y and z-axis $\Delta_{\alpha y}$ and $\Delta_{\alpha z}$. Deformations resulted from the equivalent gravity is shown in Fig. 8. Before optimization, the maximum deformations of T5 PKM resulted from gravity are $\Delta_{lx} = 0.6291$mm, $\Delta_{\alpha y} = -0.8717 \times 10^{-3}$rad, $\Delta_{\alpha z} = -0.7356 \times 10^{-4}$rad. They become 0.2667 mm, -0.3574×10^{-3}rad and -0.3156×10^{-4}rad after optimization. The comparison shows that deformations after optimization are approximately 0.4 to 0.5 times of the values before optimization. It indicates that the effects of gravity have been greatly reduced after optimization.

6. Conclusion

Stiffness and mass are basic and important performances for PKMs. They often restrict each other. In order to fully reflect their competitive features and achieve cooperative equilibrium, a stiffness and mass optimization method is proposed in this paper. The conclusions are drawn as follows.

(1) Both overall and worst-case stiffness indices are defined on the basis of instantaneous energy. It has consistent units and clear physical meaning. Mass index is defined by the PKM dimensions. Relying on RSM, the analytical mapping models of the performance indices are formulated. By applying these analytical models, the efficiency of optimization will be improved while the accuracy is assured.
(2) Parameter uncertainty is unavoidable due to the machining and assembling errors during construction. Random samples are applied to model the parameter uncertainty. Based on safety factors, PSF is defined to evaluate the effects of parameter uncertainty to the optimization problem. Then constraint conditions are established by the PSFs. The consideration of parameter uncertainty makes the optimization more realistic thus the physical prototype becomes more reliable.
(3) The multi-objective optimization is implemented by PSO. From the obtained Pareto frontier, the cooperative equilibrium point is selected to reach the best compromise among stiffness and mass indices. T5 PKM is chosen as an example to demonstrate the optimization approach. The result show that mass increases 17.17% but the stiffness is nearly 3 times bigger than before optimization. A satisfactory compromise between stiffness and mass performances are achieved.

Acknowledgment

This research work was supported by the National Natural Science Foundation of China (NSFC) under Grant Nos. 51475321 and 51675366, Tianjin Research Program of Application Foundation and Advanced Technology under Grant Nos. 15JCZDJC38900 and 16JCYBJC19300, and International Postdoctoral Exchange Fellowship Program 2017 by the Office of China Postdoctoral Council.

References

[1] H.F. Ding, P. Huang, J.F. Liu, A. Kecskeméthy, Automatic structural synthesis of the whole family of planar 3-degrees of freedom closed loop mechanisms, J. Mech. Robot. 5 (4) (2013) 041006-1-041006-10.
[2] D. Wang, R. Fan, W.Y. Chen, Performance enhancement of a three-degree-of-freedom parallel tool head via actuation redundancy, Mech. Mach. Theory 71 (2014) 142–162.
[3] F.G. Xie, X.J. Liu, C. Wang, Design of a novel 3-dof parallel kinematic mechanism: type synthesis and kinematic optimization, Robotica 33 (3) (2015) 622–637.
[4] J. Wu, B.B. Zhang, L.P. Wang, A measure for evaluation of maximum acceleration of redundant and nonredundant parallel manipulators, J. Mech. Robot. 8 (2) (2016) 021001-1-021001-8.
[5] Q.C. Li, Z. Chen, Q.H. Chen, C.Y. Wu, H.D. Hu, Parasitic motion comparison of 3-prs parallel mechanism with different limb arrangements, Robot. Com.-Int. Manuf. 27 (2) (2011) 389–396.
[6] A.B.K. Rao, P.V.M. Rao, S.K. Saha, Dimensional design of hexaslides for optimal workspace and dexterity, IEEE Trans. Robot. 21 (3) (2005) 444–449.
[7] F. Gao, B.B. Peng, H. Zhao, W.M. Li, A novel 5-dof parallel kinematic machine tool, Int. J. Mach. Tools Manuf. 31 (2006) 201–207.
[8] C. Fan, G.L. Zhao, J. Zhao, L. Zhang, L.N. Sun, Calibration of a parallel mechanism in a serial-parallel polishing machine tool based on genetic algorithm, Int. J. Adv. Manuf. Tech. 81 (2015) 27–37.
[9] Y.M. Song, Q. Yang, G. Dong, T. Sun, Type synthesis of 2-dof rotational parallel mechanism actuating the inter-satellite link antenna, Chin. J. Aeronaut. 29 (6) (2016) 1795–1805.
[10] F. Pierrot, V. Nabat, O. Company, S. Krut, P. Poiget, Optimal design of a 4-dof parallel manipulator: from academia to industry, IEEE Trans. Robot. 25 (2009) 213–224.
[11] J.P. Merlet, D. Daney, appropriate design of parallel manipulators, in: Smart Devices and Machines for Advanced Manufacturing, Springer, London, 2008, pp. 1–25.
[12] Z. Gao, D. Zhang, Y.J. Ge, Design optimization of a spatial six degree-of-freedom parallel manipulator based on artificial intelligence approaches, Robot. Com.-Int Manuf. 26 (2010) 180–189.
[13] B.H. Kang, J.T.Y. Wen, N.G. Dagalakis, J.J. Gorman, Analysis and design of parallel mechanisms with flexure joints, IEEE Trans. Robot. 21 (6) (2005) 1179–1185.
[14] Z.M. Bi, L.H. Wang, Optimal design of reconfigurable parallel machining systems, Robot. Com.-Int Manuf. 25 (2009) 951–961.
[15] H.P. Shin, S.C. Lee, J.I. Jeong, J.W. Kim, Antagonistic stiffness optimization of redundantly actuated parallel manipulators in a predefined workspace, IEEE/ASME Trans. Mech. 18 (3) (2013) 1161–1169.
[16] Z. Gao, D. Zhang, Performance analysis, mapping and multiobjective optimization of a hybrid robotic machine tool, IEEE Trans. Int. Electron. 62 (1) (2015) 423–433.
[17] S.S. Rao, Y Hu, Multi-objective optimal design of stationary flat-plate solar collectors under probabilistic uncertainty, J. Mech. Des. 132 (2010) 094501-1-094501-6.
[18] R. Kelaiaia, O. Company, A. Zaatri, Multi-objective optimization of a linear delta parallel robot, Mech. Mach. Theory 50 (2012) 159–178.
[19] P.A. Voglewede, I. Ebert-Uphoff, Overarching framework for measuring closeness to singularities of parallel manipulators, IEEE Trans. Robot. 21 (6) (2005) 1037–1045.
[20] J. Wu, L.P. Wang, L.W. Guan, A study on the effect of structure parameters on the dynamic characteristics of a prrrp parallel manipulator, Nonlinear Dyn. 74 (2013) 227–235.
[21] C. Menon, R. Vertechy, M.C. Markot, V. Parenti-Castelli, Geometrical optimization of parallel mechanisms based on natural frequency evaluation: application to a spherical mechanism for future space applications, IEEE Trans. Robot. 25 (1) (2009) 12–24.
[22] C. Alessandro, S. Rosario, Elastodynamic optimization of a 3t1r parallel manipulator, Mech. Mach. Theory 73 (2014) 184–196.
[23] R. Kelaiaia, A. Zaatri, O. Company, Multiobjective optimization of 6-dof ups parallel manipulators, Adv. Robotics 26 (2012) 1885–1913.
[24] R. Ur-Rehman, S. Caro, D. Chablat, P. Wenger, Multiobjective design optimization of 3-prr planar parallel manipulators, in: 20th CIRP Design conference, Nantes, France, 2010, pp. 1–10.

[25] G.L. Wu, S. Caro, S.P. Bai, J. Kepler, Dynamic modeling and design optimization of a 3-dof spherical parallel manipulator, Robot Auton. Syst. 62 (2014) 1377–1386.
[26] A. Khakhali, N. Nariman-zadeh, A. Darvizeh, A. Masoumi, B. Notghi, Reliability-based robust multi-objective crashworthiness optimization of s-shaped box beams with parametric uncertainties, Int. J. Crashworthines 15 (4) (2010) 443–456.
[27] J.G. Fang, Y.K. Gao, G.Y. Sun, Q. Li, Multiobjective reliability-based optimization for design of a vehicle door, Finite Elem. Anal. Des. 67 (2013) 13–21.
[28] S.-D. Stan, R. Balan, Maties, Multi-objective design optimization of mini parallel robots using genetic algorithms, in: IEEE International Symposium on Industrial Electronics, Vigo, Spain, 2007, pp. 2173–2178.
[29] Y. Yun, Y.M. Li, Optimal design of a 3-PUPU parallel robot with compliant hinges for micromanipulation in a cubic workspace, Robot. Com.-Int Manuf. 27 (6) (2011) 977–985.
[30] A.R. Shirazi, M.M.S. Fakhrabadi, A. Ghanbari, Optimal design of a 6-dof parallel manipulator using particle swarm optimization, Adv. Robotics 26 (13) (2012) 1419–1441.
[31] D. Zhang, Z. Gao, Forward kinematics, performance analysis, and multi-objective optimization of a bio-inspired parallel manipulator, Robot. Com.-Int Manuf. 28 (4) (2012) 484–492.
[32] H. Wang, L.S. Zhang, G.L. Chen, S.Z. Huang, Parameter optimization of heavy-load parallel manipulator by introducing stiffness distribution evaluation index, Mech. Mach. Theory 108 (2017) 244–259.
[33] R.Z. Wang, X.M. Zhang, Optimal design of a planar parallel 3-dof nanopositioner with multi-objective, Mech. Mach. Theory 112 (2017) 61–83.
[34] U. Baumgartner, C. Magele, W. Renhart, Pareto optimality and particle swarm optimization, IEEE Tran. Mag. 40 (2) (2004) 1172–1175.
[35] M. Ceccarelli, G. Carbone, A stiffness analysis for capaman (cassino parallel manipulator), Mech. Mach. Theory 37 (5) (2002) 427–439.
[36] Z. Gao, D. Zhang, X. Hu, Y. Ge, Design, analysis, and stiffness optimization of a three degree of freedom parallel manipulator, Robotica 28 (2010) 349–357.
[37] Q. Xu, Y. Li, An investigation on mobility and stiffness of a 3-dof translational parallel manipulator via screw theory, Robot. Com.-Int Manuf. 24 (3) (2008) 402–414.
[38] A. Rezaei, A. Akbaradeh, M-R. Akbarzadeh-T, An investigation on stiffness of a 3-psp spatial parallel mechanism with flexible moving platform using invariant form, Mech. Mach. Theory 51 (2012) 195–216.
[39] T. Sun, H. Wu, B.B. Lian, Y. Qi, P.F. Wang, Y.M. Song, Stiffness modeling, analysis and evaluation of a 5 degree of freedom hybrid manipulator for friction stir welding, in: Proc. IMechE. Part C: J Mechanical Engineering Science, 2016, doi:10.1177/0954406216668911.
[40] K.C. Olds, Global indices for kinematic and force transmission performance in parallel robots, IEEE Trans. Robotic. 31 (2) (2015) 494–500.
[41] A. Witek-Krowiak, K. Chojnacka, D. Podstawczyk, A. Dawiec, K. Pokomeda, Application of response surface methodology and artificial neural network methods in modelling and optimization of biosorption process, Bioresource Technol 160 (2014) 150–160.
[42] R. Jin, W. Chen, T.W. Simpson, Comparative studies of metamodeling techniques under multiple modeling criteria, Struct. Multidisc. Optim. 23 (2001) 1–13.
[43] L. Liao, Discovering prognostic features using genetic programming in remaining useful life prediction, IEEE Trans. Ind. Electron. 61 (5) (2014) 2464–2472.
[44] Y.M. Song, B.B. Lian, T. Sun, G. Dong, Y. Qi, H. Gao, A novel five-degree-of-freedom parallel manipulator and its kinematic optimization, J. Mech. Rob. 6 (4) (2014) 041008-1-041008-9.
[45] B.B. Lian, T. Sun, Y.M. Song, Y. Jin, M. Price, Stiffness analysis and experiment of a novel 5-dof parallel kinematic machine considering gravitational effects, Int. J. Mach. Tools. Manuf. 95 (2015) 82–96.
[46] B.B. Lian, T. Sun, Y.M. Song, Parameter sensitivity analysis of a 5-dof parallel manipulator, Robot. Com.-Int Manuf. 46 (2017) 1–14.